JOURNAL OF THERMOPHYSICS AND HEAT TRANSFER
Vol. 24, No. 2, April–June 2010

Transient Analysis of Cryogenic Liquid-Hydrogen Storage Tank with Intermittent Forced Circulation

Son H. Ho*
University of Central Florida, Orlando, Florida 32816
and
Muhammad M. Rahman†
University of South Florida, Tampa, Florida 33620

DOI: 10.2514/1.41135

This paper presents the transient analysis of fluid flow and heat transfer in a zero-boil-off cryogenic storage tank of liquid hydrogen. The system includes a tank with a cylindrical wall and oblate spheroidal top and bottom, a heat pipe located along the symmetric axis of the tank, and an active circulator consisting of a pump-motor assembly and a spray nozzle. Whenever the maximum temperature inside the tank reaches the boiling point under the working pressure in the tank, the pump is activated to create a forced flow at the nozzle to cool down the heated fluid. After a preset interval of 1 h, the pump is shut down and goes on standby until the maximum temperature reaches its threshold again, and then the pump starts a new cycle. The transient simulation allows the visualization of flow-field and temperature distributions, as well as the computation of maximum and mean temperatures of the fluid in various stages of the pump cycle. This information reveals insights into the characteristics of the stored liquid hydrogen and can assist in optimizing the location of temperature sensors, which provide input to the control system.

Nomenclature

A–C	=	geometric dimensions of liquid-hydrogen storage system, m
c_p	=	specific heat, J/kg K
D–H	=	geometric dimensions of liquid-hydrogen storage system, m
k	=	thermal conductivity, W/m K
k_t	=	eddy or turbulent thermal conductivity, W/m K
L	=	geometric dimension of liquid-hydrogen storage system, m
l_c	=	characteristic length scale, m
l_m	=	mixing length, m
l_n	=	distance from the nearest wall, m
M–N	=	geometric dimensions of liquid-hydrogen storage system, m
n	=	coordinate in direction normal to boundary surface, m
P	=	geometric dimension of liquid-hydrogen storage system, m
Pr_t	=	turbulent Prandtl number
p	=	pressure, Pa
q_w	=	heat flux on tank wall, W/m^2
R	=	geometric dimension of liquid-hydrogen storage system, m
r	=	radial coordinate, m
S_k	=	nominal element size on boundary edges ($k = 1, 2, 3$), m
T	=	temperature, K
T_c	=	temperature on the surface of the evaporator section of the heat pipe, K
$T_{\max}$	=	maximum temperature, K
T_{mean}	=	mean temperature, K
t	=	time, s
u	=	velocity, m/s
u_i, u_j	=	generalized velocity in tensor notation, m/s
V	=	fluid speed at nozzle, m/s
x_i, x_j	=	generalized coordinates in tensor notation, m
z	=	axial coordinate, m

Greek symbols

θ	=	azimuthal coordinate
κ	=	von Karman constant
μ	=	viscosity, Pa s
μ_t	=	eddy or turbulent viscosity, Pa s
ρ	=	fluid density, kg/m^3
σ	=	fluid stress, Pa

Subscripts

r	=	in r-direction
z	=	in z-direction
θ	=	in θ-direction

Received 21 September 2008; revision received 4 October 2009; accepted for publication 18 October 2009.

*Postdoctoral Associate; Department of Mechanical, Materials, and Aerospace Engineering. Member AIAA
†Professor, Department of Mechanical Engineering.

I. Introduction

HYDROGEN has been recognized as a powerful and clean fuel for a few decades for space applications [1], and recently for general transportation such as automobiles [2]. Hydrogen has been identified to play a key role as an energy source in the future. Although hydrogen has many advantages over most conventional fuels, efficient storage of hydrogen is difficult because of its very low gaseous density [3]. Liquid storage has a substantial advantage over gaseous or chemical storage because of its much lower storage volume for the same mass of stored hydrogen. However, a conventional cryogenic storage tank suffers from the loss of hydrogen due to the boil-off of the cryogen, induced by heat leakage into the tank from the warmer surrounding environment. Boil-off results in increasing the amount of gaseous hydrogen thus increasing the pressure in the closed tank. To maintain the inner pressure within the structural limits of the tank, the stored cryogen needs to be periodically vented.

The zero-boil-off (ZBO) concept has evolved as an innovative means of pressure control in storage tanks by a synergistic application of passive insulation, active heat removal, and forced mixing within the tank. The goal is to store the hydrogen fuel for a very long

time without loss. In recent years, a number of efforts have been made towards the development of cryogenic storage systems with the ZBO concept. Hastings et al. [4] presented an overview of the development of ZBO storage systems at NASA, showing that a ZBO system has mass advantage over passive storage. Kittel [5] suggested an alternative approach for the long-term storage of cryogenic propellants using a reliquefier that uses the propellant vapor as the working fluid. Salerno and Kittel [6] presented a proposed Mars reference mission and concomitant cryogenic fluid-management technology with a combination of both active and passive technologies to satisfy a wide range of requirements. Hofmann [7] presented a theory of boil-off gas-cooled shields for cryogenic storage vessels using an analytical method to determine the effectiveness of intermediate refrigeration. Haberbusch et al. [8] developed a design tool for a thermally densified ZBO cryogen storage system for space applications. The model predicted that a ZBO densified liquid-hydrogen storage system reduces the overall storage-system mass and volume. Wilson et al. [9] did a study with the goal of storing liquid hydrogen in space in a linerless composite tank for a period of 20 years with a 2% boil-off loss. Kamiya et al. [10,11] presented the development of a large experimental apparatus to measure the thermal conductance of various types of insulation and used that for the testing of insulation structures. The apparatus could test specimen with dimensions up to 1.2 m diameter and 0.3 m thickness. Different insulation structures were tested, one with vacuum multilayer insulation (MLI) and glass-fiber reinforced plastic (GFRP), and another having vacuum solid insulation. Venkat and Sherif [12] studied a liquid-storage system under normal and reduced-gravity conditions.

Mukka and Rahman [13,14] used computational fluid dynamics (CFD) simulation to study the fluid flow and heat transfer in a cryogenic liquid-hydrogen storage tank where cool fluid enters the tank at one end, mixes with hot fluid, and exits at the other end. Rahman and Ho [15] studied the steady-state fluid flow and heat transfer in a closed ZBO cryogenic storage tank with a heat pipe surrounded by an array of many pump-nozzle units as an artificial circulatory system. The numerical simulations were done using an axisymmetric model because of the nearly axisymmetric nature of the problem. Subsequently, Ho and Rahman [16] presented a parametric analysis using a three-dimensional model for steady-state fluid flow and heat transfer in a similar storage tank with a single pump-nozzle unit, focusing on the effect of the normal speed at the nozzle face. The heat-pipe mixer (pump) design concept was first introduced by Plachta [17] as another ZBO design concept implemented within a prototype developed at NASA–Glenn Research Center. The prototype system included a spherical tank for liquid nitrogen with a heat pipe that had many fins on the evaporator section and a submerged mixer pump that collected and directed the fluid toward the heat-pipe fins. The experimental results showed that the prototype performed better than expected and that it was promising for future missions.

This paper presents the transient analysis of fluid flow and heat transfer in a ZBO cryogenic storage system of liquid hydrogen. The study considers a cylindrical tank with spheroidal top and bottom as shown in Fig. 1a. The tank wall is made of aluminum, and a multilayered blanket of cryogenic insulation (MLI) has been attached to the external wall of the aluminum. The tank is connected to a cryocooler via a heat pipe to dissipate the heat that leaks through the insulation and the tank wall into the fluid within the tank. The condenser section of the heat pipe dissipates heat to the cryocooler while the evaporator section picks up heat from the fluid within the tank. The hot fluid is directed to the evaporator section of the heat pipe using a fluid-circulation system within the tank. This system consists of a pump, a spray head for the discharge of the fluid, and a collector tube feeding the pump. Normally, the pump does not work until the maximum temperature inside the tank reaches a threshold, which is the boiling temperature of liquid hydrogen under the working pressure of the tank. When the fluid reaches the temperature threshold, the pump starts to run and discharge the heated fluid on the colder surface of the evaporator section of the heat pipe and thus cools the fluid. After a specified time interval, the pump shuts off and stands by until the fluid reaches the threshold again.

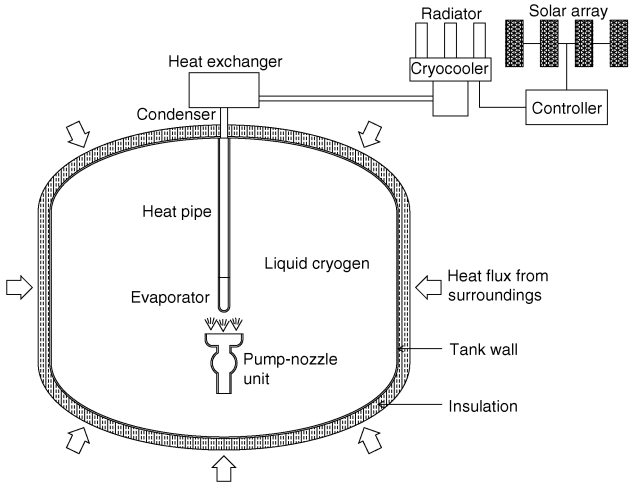

a) Schematic diagram of storage system

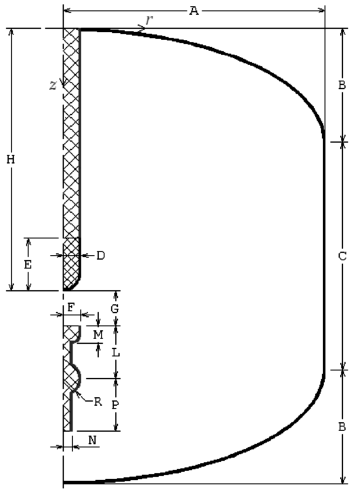

b) Axisymmetric model and generic dimensions

Fig. 1 Cryogenic liquid-hydrogen storage system.

Only the fluid inside the tank is modeled for computation. The symmetry of the computational domain suggests the use of an axisymmetric model, which consumes fewer computing resources as compared with that required for solving the original three-dimensional problem. An axisymmetric model of the fluid inside the storage tank is presented in Fig. 1b. The essential dimensions are denoted in general form by capital letters. The axis of the tank is shown as the centerline coincident with the z-axis. The origin of the coordinate system is located at the topmost point in the tank as shown in Fig. 1b. The cylindrical wall and the spheroidal top and bottom are shown as a straight line and two elliptical arcs. The heat pipe is located along the centerline and has three sections: the tip (evaporator section), whose surface is kept at a constant low temperature; the handle, which is considered adiabatic; and the condenser section, located outside the tank. It may be noted that the present investigation focused on fluid motion within the tank and did not consider any details on the operation of the heat pipe or the cryocooler. Related experimental studies by Plachta [17] and Christie et al. [18] demonstrated the operation of the heat pipe and the cyrocooler for ZBO storage of liquid nitrogen. It is expected that a similar system will be used for ZBO storage of liquid hydrogen.

II. Mathematical Model

To describe the fluid flow and heat transfer of liquid hydrogen inside the tank, it is necessary to determine the distributions of velocity and temperature in the entire domain by solving the

equations for the conservation of mass, momentum, and energy. It is assumed that the tank is filled with liquid cryogen. For transient incompressible flow, the equations for the conservation of mass and momentum can be written as [19]:

$$\frac{1}{r}\frac{\partial}{\partial r}(ru_r) + \frac{\partial u_z}{\partial z} = 0 \tag{1}$$

$$\rho\left(\frac{\partial u_r}{\partial t} + u_r\frac{\partial u_r}{\partial r} + u_z\frac{\partial u_r}{\partial z}\right) = \frac{1}{r}\frac{\partial}{\partial r}(r\sigma_{rr}) - \frac{\sigma_{\theta\theta}}{r} + \frac{\partial \sigma_{rz}}{\partial z} \tag{2}$$

$$\rho\left(\frac{\partial u_z}{\partial t} + u_r\frac{\partial u_z}{\partial r} + u_z\frac{\partial u_z}{\partial z}\right) = \frac{1}{r}\frac{\partial}{\partial r}(r\sigma_{rz}) + \frac{\partial \sigma_{zz}}{\partial z} \tag{3}$$

where

$$\sigma_{rr} = -p + 2(\mu + \mu_t)\frac{\partial u_r}{\partial r} \tag{4}$$

$$\sigma_{\theta\theta} = -p + 2(\mu + \mu_t)\frac{u_r}{r} \tag{5}$$

$$\sigma_{rz} = (\mu + \mu_t)\left(\frac{\partial u_r}{\partial z} + \frac{\partial u_z}{\partial r}\right) \tag{6}$$

$$\sigma_{zz} = -p + 2(\mu + \mu_t)\frac{\partial u_z}{\partial z} \tag{7}$$

It should be noted that no buoyancy term has been added in the momentum equation. The primary motivation of the study is to address the long-term storage of cryogens in space, where gravity and hence buoyancy is negligible. Assuming that there is no heat generation and that viscous dissipation and pressure work are negligible, the equation for the conservation of energy can be written as

$$\rho c_p\left(\frac{\partial T}{\partial t} + u_r\frac{\partial T}{\partial r} + u_z\frac{\partial T}{\partial z}\right) = \frac{1}{r}\frac{\partial}{\partial r}\left[(k + k_t)r\frac{\partial T}{\partial r}\right] + \frac{\partial}{\partial z}\left[(k + k_t)\frac{\partial T}{\partial z}\right] \tag{8}$$

For modeling turbulent flow, the effective viscosity is defined as the sum of the dynamic viscosity (physical property) and an eddy viscosity μ_t representing the effects of turbulent flow. Similar treatment is also applied for the effective thermal conductivity with an additional turbulent thermal conductivity k_t. Details of turbulence modeling can be found in textbooks on convective heat transfer such as Kays et al. [19]. Turbulent or eddy viscosity can be estimated by using the general mixing-length model given in tensor notation form by Rodi [20] as

$$\mu_t = \rho l_m^2\sqrt{\left(\frac{\partial u_i}{\partial x_j} + \frac{\partial u_j}{\partial x_i}\right)\frac{\partial u_i}{\partial x_j}} \tag{9}$$

where

$$l_m = \min\{\kappa l_n, 0.09 l_c\} \tag{10}$$

and $\kappa \approx 0.41$. Turbulent thermal conductivity can be estimated as

$$k_t = \frac{c_p \mu_t}{Pr_t} \tag{11}$$

where $Pr_t \approx 0.85$. To completely define the problem, appropriate boundary conditions are required on every boundary segment of the computational domain. For the continuity and the momentum equations, the boundary conditions on velocity can be written thus:

$$\text{On the nozzle face}: u_r = 0, \qquad u_z = V \tag{12}$$

$$\text{On the centerline}: u_r = 0, \qquad \frac{\partial u_z}{\partial r} = 0 \tag{13}$$

$$\text{On all solid surfaces}: u_r = 0, \qquad u_z = 0 \tag{14}$$

For the energy equation, the boundary conditions on temperature can be written thus:

$$\text{On the tank wall}: k\frac{\partial T}{\partial n} = q_w \tag{15}$$

$$\text{On the evaporator section}: T = T_c \tag{16}$$

$$\text{On other boundary surfaces}: \frac{\partial T}{\partial n} = 0 \tag{17}$$

The dimensions for the axisymmetric model shown in Fig. 1b are set as follows: A = 1.50 m, B = 0.65 m, C = 1.30 m, D = 0.10 m, E = 0.30 m, F = 0.05 m, G = 0.20 m, H = 1.50 m, L = 0.30 m, M = 0.10 m, N = 0.05 m, P = 0.30 m, and R = 0.10 m. The tank dimensions correspond to a hydrogen storage tank used by NASA for demonstration of multilayer insulation and a cryocooler.

The fluid properties are taken as constant as follows: $\rho = 70$ kg/m^3, $\mu = 12 \times 10^{-6}$ Pa s, $c_p = 10$ kJ kg^{-1} K^{-1}, and $k = 0.1$ W m^{-1} K^{-1}. A constant heat flux, $q_w = 1$ W/m^2, is applied on the heated surfaces of the wall. The magnitude of heat flux was approximated from typical heat leakage in insulated cryogenic storage systems. A constant temperature, $T_c = 20$ K, is assumed on the evaporator section of the heat pipe. It is assumed that initially the fluid inside the tank has a uniform temperature distribution of 20 K. The operating pressure in the tank is 2 atm (203 kPa). Therefore, to prevent boil-off, the maximum temperature inside the tank cannot exceed the boiling point at 2 atm (23 K). The velocity at the nozzle is defined as

$$V = \begin{cases} 0.08 \text{ m/s} & \text{start when } \max(T) = 23 \text{ K, run for 1 hour then stop} \\ 0 & \text{otherwise} \end{cases} \tag{18}$$

III. Numerical Solution

The governing equations, including the mixing length turbulence model along with the boundary conditions [Eqs. (1–18)], were solved using the finite-element method. The CFD analysis software package FIDAP [21] was used for this purpose. In each element, velocity components, pressure, and temperature were approximated using the Galerkin procedure [22], which led to a set of algebraic equations that defined the discretized continuum. Four-node quadrilateral elements were used. Layers of regular elements of higher density were assigned along the solid surfaces where high rates of momentum and heat transfer exist. A mesh with approximately 10,200 elements was used. The fully coupled successive substitution algorithm was used to solve the nonlinear system of equations. Two convergence criteria were used: the relative errors of the solutions and the residuals of the nonlinear equations. The relative error criterion was reached when the relative error at an iteration was less than a specified tolerance. The residual criterion checked whether the ratio of the residual vector at an iteration to a reference residual vector was less than another specified tolerance. The iterative procedure was considered converged when both criteria were satisfied. The

tolerances for the present simulations were 0.0001 and 0.01 for relative error and residual, respectively.

For all simulations, meshes of four-node quadrilateral elements were used. The mesh-generation software GAMBIT [23] was used for this purpose. The size of the mesh was controlled by adjusting the element size on the boundary edges of solid–fluid interfaces. Because of the complexity of the geometry, three nominal element sizes were used for three groups of boundary segments. The first element size S_1 was used for large-size boundary segments such as those that form the tank wall and the adiabatic section of the heat pipe. The second element size S_2 was for medium-size boundary segments, which form the evaporator section of the heat pipe. The third element size S_3 was for small-size boundary segments such as inlet and outlet openings. Each boundary segment was meshed by using a uniform meshing scheme. The height of the element layers adjacent to the solid–fluid interface increased inward by a factor of 1.2, starting with S_3 at the interface. These layers of structured mesh of smaller-size elements covered the regions having high rates of momentum and heat transfer. Beyond these layers, the rest of the computational domain was covered with an unstructured mesh of quadrilateral elements.

The distribution of element size in the computational domain was determined from a mesh-independence study by systematically changing the mesh density in all spatial directions, both globally and locally, to obtain a mesh that gave a numerical solution independent of the number of elements with a temperature accuracy of ± 0.02 K. The final set of mesh sizes were $S_1 = 0.02$ m, $S_2 = 0.01$ m, and $S_3 = 0.005$ m. For the mesh independence study, different cases of mesh size were considered. Taking the final set of mesh sizes as the reference, steady-state simulations were performed using 16, 8, 4, 2, 1.5, 1.25, 1 (reference), and 0.75 times the reference mesh size, or 100, 275, 908, 2783, 4962, 6847, 10,209 (reference), and 17,408 quadrilateral elements. Figure 2 shows how the representative fluid temperature in the tank became independent of the mesh size as the number of elements increased (the element size decreased). Figure 2 presents the values of maximum temperature, average temperature, and temperatures at three locations as functions of the number of elements. This demonstrates that as the number of elements increased over 10,000, mesh independence of the numerical solution was achieved. The mesh with 10,209 elements was found quite adequate for accurate numerical prediction. Therefore, this reference set of mesh sizes was used for generating the meshes for all simulations presented in this paper.

IV. Results and Discussion

The solution obtained by solving the governing equations associated with their boundary conditions and the initial condition gives the spatial distributions of four primary variables as functions of time: two velocity components (axial and radial), pressure, and temperature distributed over the entire computational domain. The transient solution can be presented in several stages. Initially, the fluid is stationary and has a uniform temperature of 20 K. In stage 1, the stagnant fluid is heated by conduction only, until the maximum temperature reaches 23 K. In stage 2, the pump starts a 1-h run and creates forced flow from the nozzle; heat transfer includes conduction and convection. In stage 3, the pump stops, but there is still fluid flow as the result of stage 2. Heat transfer also includes conduction and convection until the entire body of fluid becomes stationary after a long-enough time. Stages 2 and 3 compose a cycle with a run interval (stage 2) and rest interval (stage 3). The following cycles are similar to the first one.

Figure 3 presents the temperature distribution at the end of stage 1 (after 83 h) when the maximum temperature reaches 23 K. It shows the conduction pattern with temperature decreasing gradually from the heated surface (tank wall) toward the cold surface (evaporator section of the heat pipe) and separating into isothermal layers. It can be observed that the inner isothermal layers tend to round off at the corners of the tank, shared by the cylindrical shell and the spheroidal top and bottom, with more uniform changes of curvature. Thus the geometric shape of the tank is not *thermally conformal* at the corners. The spots that have maximum temperature are located at these corners. A sensor is needed at one of these locations to monitor the temperature there and give a signal to turn on the pump if the temperature exceeds a specified threshold (23 K). That finishes stage 1. Figure 4 shows the changes in maximum and mean temperatures of the fluid in stage 1 as functions of time. The mean temperature increases linearly while the maximum temperature increases at a higher rate in nonlinear fashion, especially during the first several hours.

Figures 5 and 6 present the distributions of fluid flow and temperature at the beginning ($t = 5$ minutes) and at the end ($t =$ 60 minutes) of stage 2, respectively. In Fig. 5a, the fluid discharged from the nozzle reaches the evaporator section, cools off the fluid along the way, and flows along the length of the heat pipe up to the top of the tank. Then, this fluid stream follows the curvature of the tank shell, sweeping through the top and back down the cylindrical outer shell, increasing the heat transfer at the tank wall. The lower part of the tank is still undisturbed, making it harder for the flow to displace the stagnant fluid there due to the lack of momentum of the flow, since it is far away from the nozzle. The flow is forced to separate from the wall and move toward the suction tube of the pump, making a closed streamline. The fluid enclosed by the streamline is directly driven by the jet from the nozzle and affected by viscous forces. That creates a family of streamlines in the region. As a result of such a flow pattern, the temperature distribution shown in Fig. 5b has a high-temperature region next to the bottom and gradually decreases upwardly and inwardly from the lower corner of the tank. The location of maximum temperature moves from the lower corner toward the bottom. After 1 h of running the pump, the velocity field is close to steady state and

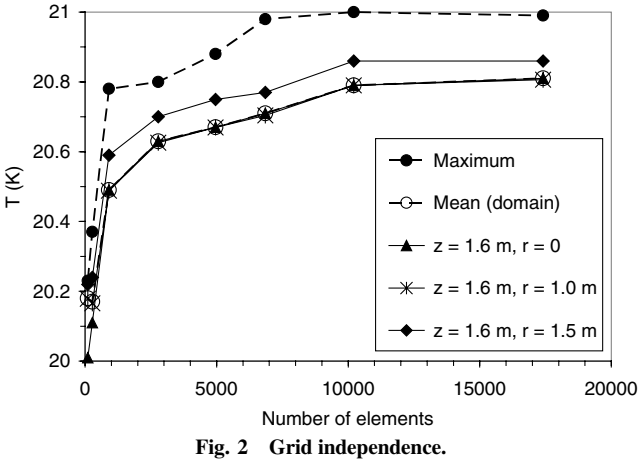

Fig. 2 Grid independence.

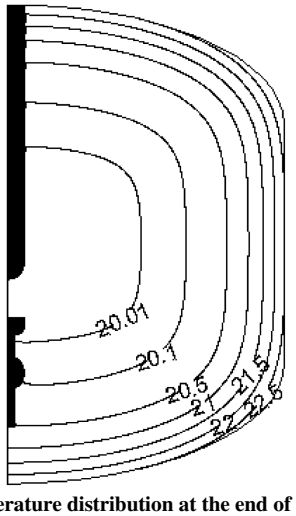

Fig. 3 Temperature distribution at the end of stage 1, T (K).

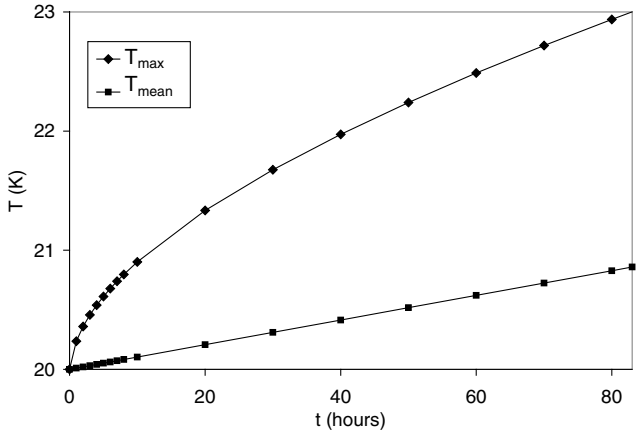

Fig. 4 Maximum and mean temperatures vs elapsed time, stage 1.

has the distribution shown in Fig. 6a. The fluid mixing is better, resulting in a much more uniform temperature field as shown in Fig. 6b where the high-temperature region is pressed to the wall and remains in a thin layer. The location of maximum temperature is now at the center of the bottom (on the centerline) where there is a stagnant spot since the fluid flow collected by the suction tube cannot reach that spot. Stage 2 ends when the pump shuts down.

For quantitatively assessing the effect of fluid mixing by the pump on the temperature distribution, Fig. 7 shows how the maximum and mean temperatures decrease over time. The mean temperature decreases gradually. The maximum temperature decreases slowly at first, then drops at a higher rate, and then slows down at the end. The drop in the maximum temperature for this stage is about 2 K in 1 h.

Figure 8 shows the temperature distribution at the end of stage 3. The pattern is different than that at the end of stage 1 (Fig. 3) since there is still slow circulation remaining, even though the pump has been off for some time. Thus, convective heat transfer makes stage 3 different from stage 1. The location of maximum temperature in this situation is at half of the height of the cylindrical shell on the tank wall. This location is where the temperature must be measured by another sensor in order to switch on the pump every time the temperature there exceeds the threshold of 23 K.

Figure 9 presents the maximum and mean temperatures during stage 3, which are similar to those of stage 1 (Fig. 4) although the numerical values are different. The mean temperature still increases linearly and the maximum temperature increases nonlinearly, with a fast rate at the beginning then slowing down. However, it takes only about 70 h for the fluid to heat up to a maximum temperature of 23 K again (compared with 83 h in stage 1). This happens because the

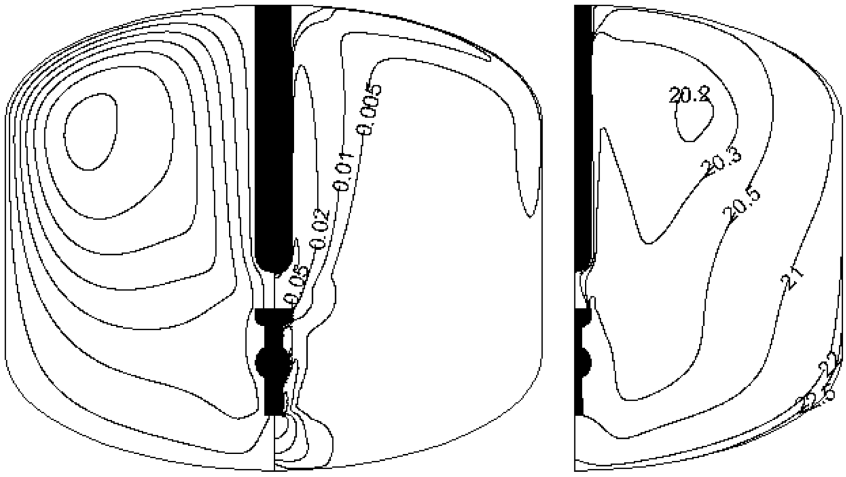

a) Streamlines (left half) and speed, u (m/s) (right half) **b) Temperature, T(K)**

Fig. 5 Distributions of velocity and temperature, stage 2, at $t = 5$ minutes.

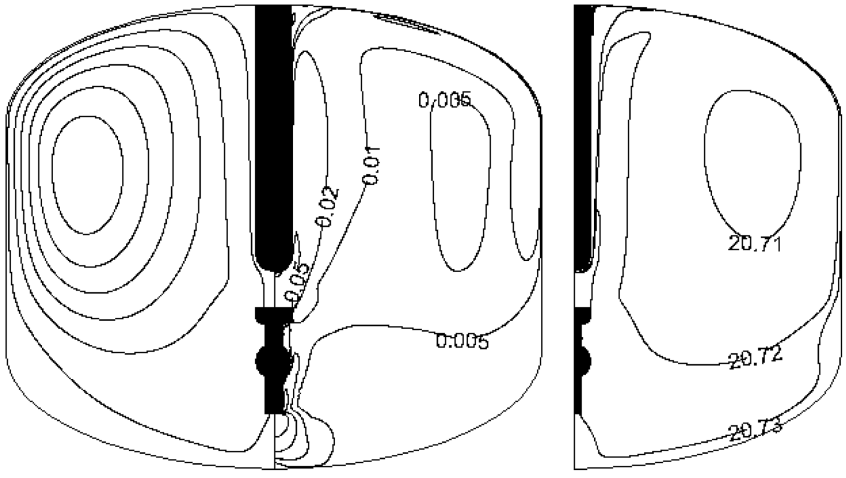

a) Streamlines (left half) and speed, u (m/s) (right half) **b) Temperature, T(K)**

Fig. 6 Distributions of velocity and temperature, stage 2, at $t = 60$ minutes.

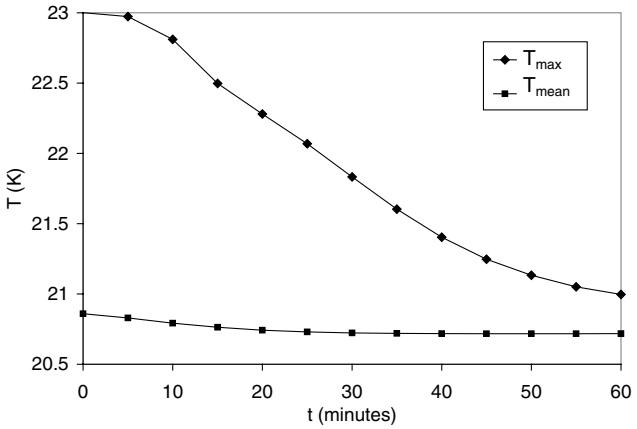

Fig. 7 Maximum and mean temperatures vs elapsed time, stage 2.

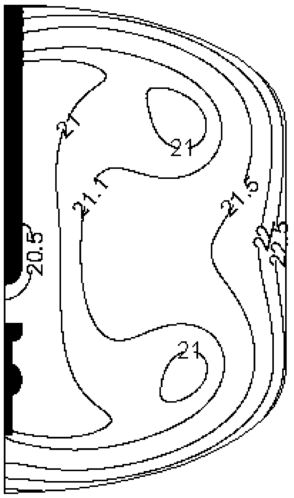

Fig. 8 Temperature distribution at the end of stage 3, *T* (K).

temperature at the beginning of stage 3 is higher than that of stage 1 as seen by comparing the mean and maximum temperatures in Figs. 4 and 9. This also implies that each of the following cycles will end at higher temperatures, and thus each cycle becomes shorter than the previous one.

Figure 10 shows the maximum and mean temperatures over several cycles. It can be observed that their behavior follows some predetermined rules. In the 1-h run interval, both representative temperatures drop but not as much as in the previous cycle. The result is that the rest interval gets shorter as the number of cycles increases.

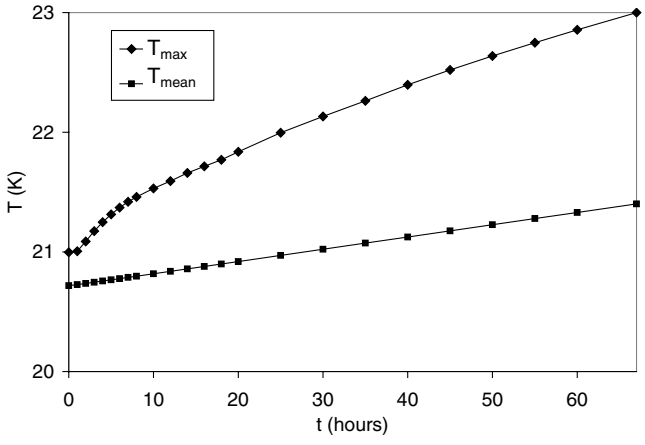

Fig. 9 Maximum and mean temperatures vs elapsed time, stage 3.

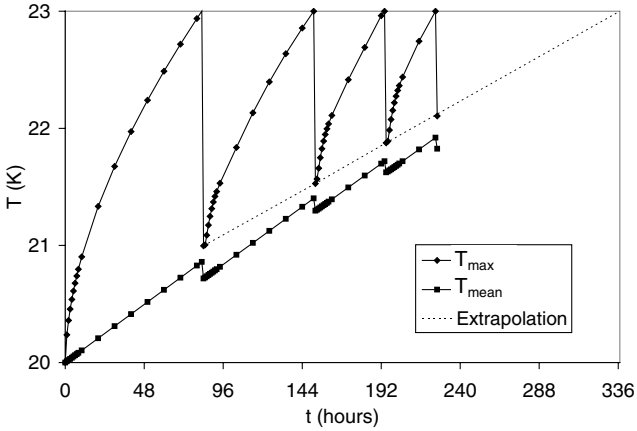

Fig. 10 Maximum and mean temperature vs elapsed time for first three cycles.

We can estimate the time when this type of cycle (1-h run interval, then rest interval until maximum temperature reaches 23 K) stops working. By extrapolating the maximum temperature at the end of each run interval, it is found that after about 337 h (14 days), the rest interval will vanish; i.e., the pump has to run for a much longer time in order to reduce the maximum temperature to a reasonable level that keeps the rest interval longer, on the order of tens of hours.

V. Conclusions

The numerical simulation presented herein provides a better understanding of the phenomena of transient fluid flow and heat transfer in an active-circulation cryogenic storage system for liquid hydrogen in space. Since there are several different flow patterns corresponding to different stages created by the intermittent operation of the pump, there are different temperature distributions that characterize each stage. As a result, the locations of the spots of maximum fluid temperature move from place to place. During stage 1, when the fluid is stagnant, the spots are at the corners of the tank. During stage 2, when the pump is running and generating strong fluid circulation, the spot is at the center of the bottom. Finally, during stage 3, when the pump is off while residual momentum maintains a weakening fluid circulation, the spot is located near the wall at half of the height of the cylindrical shell. These predictions are essential for the design of the system in terms of locating temperature sensors at the spots of highest temperature. These sensors will provide feedback to the control circuit for the operation of the pump. A pump cycle which is composed of a preset constant run interval and an upper-temperature-threshold-controlled rest interval can only work for a relatively short time (less than two weeks for the specific system considered in this study). For long-term applications, it is advisable that the run interval increase from cycle to cycle in compliance with a precomputed run interval schedule so that the pump will run long enough to keep the rest interval from being too short after a relatively long time. An alternative plan is that the run interval could be controlled by a lower-temperature threshold; i.e., instead of running for a preset interval such as 1 h as used in the simulations herein, the pump could run until the maximum fluid temperature reaches a preset lower-temperature threshold. The spot of this maximum temperature is predicted to be located at the center of the bottom of the storage tank, where another sensor will be needed for detecting the temperature. These guidelines can be very useful for designing ZBO cryogenic storage systems.

Acknowledgements

The financial support for this research was received from NASA under contract number NAG3-2751. The information provided by David Plachta at NASA–Glenn is gratefully acknowledged.

References

[1] Dawson, V. P., and Bowles, M. D., *Taming Liquid Hydrogen: The Centaur Upper Stage Rocket 1958-2002*, NASA Office of External Relations, Washington, DC, 2004.

[2] Uhrig, R. E., "Heading Toward Hydrogen: What are the Hurdles to Clean, Non-Petroleum Energy?," *Energy*, Vol. 29, No. 2, 2004, pp. 17–21.

[3] Colozza, A. J., "Hydrogen Storage for Aircraft Applications Overview," NASA CR-211867, 2002.

[4] Hastings, L. J., Plachta, D. W., Salerno, L., and Kittel, P., "An Overview of NASA Efforts on Zero Boiloff Storage of Cryogenics Propellants," *Cryogenics*, Vol. 41, Nos. 11–12, 2001, pp. 833–839. doi:10.1016/S0011-2275(01)00176-X

[5] Kittel, P., "Propellant Preservation Using Re-Liquefiers," *Cryogenics*, Vol. 41, Nos. 11–12, 2001, pp. 841–844. doi:10.1016/S0011-2275(01)00165-5

[6] Salerno, L. J., and Kittel, P., "Cryogenics and the Human Exploration of Mars," *Cryogenics*, Vol. 39, No. 4, 1999, pp. 381–388. doi:10.1016/S0011-2275(99)00043-0

[7] Hofmann, A., "Theory of Boil-off Gas Cooled Shields for Cryogenic Storage Vessels," *Cryogenics*, Vol. 44, No. 3, 2004, pp. 159–165. doi:10.1016/j.cryogenics.2003.09.003

[8] Haberbusch, M. S., Stochl, R. J., and Culler, A. J., "Thermally Optimized Zero Boil-off Densified Cryogen Storage System for Space," *Cryogenics*, Vol. 44, Nos. 6–8, 2004, pp. 485–491. doi:10.1016/j.cryogenics.2004.02.016

[9] Wilson, B., Mitchell, R., Arritt, B., Paul, C., and Hender, D., "The Feasibility of Cryogenic Storage in Space," *International SAMPE Technical Conference*, 2004, pp. 613–624.

[10] Kamiya, S., Onishi, K., Kawagoe, E., and Nishigaki, K., "A Large Experimental Apparatus for Measuring Thermal Conductance of LH2 Storage Tank Insulations," *Cryogenics*, Vol. 40, No. 1, 2000, pp. 35–44. doi:10.1016/S0011-2275(00)00005-9

[11] Kamiya, S., Onishi, K., Kawagoe, E., and Nishigaki, K., "Thermal Test of the Insulation Structure for LH2 Tank by Using the Large Experimental Apparatus," *Cryogenics*, Vol. 40, No. 11, 2000, pp. 737–748. doi:10.1016/S0011-2275(01)00031-5

[12] Venkat, S., and Sherif, S. A., "Self-Pressurization and Thermal Stratification in a Liquid Hydrogen Tank Under Varying Gravity Conditions," AIAA Paper 2004-1341, 2004.

[13] Mukka, S. K., and Rahman, M. M., "Analysis of Fluid Flow and Heat Transfer in a Liquid Hydrogen Storage Vessel for Space Applications," Space Technology and Applications International Forum Paper CP699, Feb. 2004.

[14] Mukka, S. K., and Rahman, M. M., "Computation of Fluid Circulation in a Cryogenic Storage Vessel," AIAA Paper 2004-5728, Aug. 2004.

[15] Rahman, M. M., and Ho, S. H., "Zero Boil-off Cryogenic Storage of Hydrogen," *Proceedings of the NHA 16th Annual, U. S. Hydrogen Conference*, National Hydrogen Association, Washington, DC, 2005.

[16] Ho, S. H., and Rahman, M. M., "Three-Dimensional Analysis for Liquid Hydrogen in a Cryogenic Storage Tank with Heat Pipe Pump System," *Cryogenics*, Vol. 48, Nos. 1–2, 2008, pp. 31–41. doi:10.1016/j.cryogenics.2007.09.005

[17] Plachta, D. W., "Results of an Advanced Development Zero Boil-Off Cryogenic Propellant Storage Test," Technical Report NASA TM-213390, 2004.

[18] Christie, R., Robinson, D., and Plachta, D., "Design and Operating Characteristics of a Cryogenic Nitrogen Thermosyphon," *Advances in Cryogenic Engineering: Transactions of the Cryogenic Engineering Conference*, Vol. 49, 2004, pp. 1079–1090. doi:10.1063/1.1774792

[19] Kays, W. M., Crawford, M. E., and Weigand, B., *Convective Heat and Mass Transfer*, 4th ed., McGraw Hill, New York, 2005.

[20] Rodi, W., *Turbulence Models and Their Application in Hydraulics: State-of-the-art Paper*, 2nd revised ed., International Association of Hydraulic Engineering and Research (IAHR), The Netherlands, 1984.

[21] Fluent, Inc., FIDAP 8.7.4, CFD analysis software, 2005, http://www.fluent.com/.

[22] Fletcher, C. A. J., *Computational Galerkin Methods*, Springer–Verlag, New York, 1984.

[23] Fluent, Inc., GAMBIT 2.3.16, Mesh generation software, 2006, http://www.fluent.com/.